The Effect of Solvent Variation on Structural, Optical, and Electrical Properties of TiO₂ Films Prepared by Hydrothermal Method

[1,2]Aseel S. Jasim, [2]Odai N. Salman

[1]Biomass Energy Department, Al-Nahrain Renewable Energy Research Center, Al-Nahrain University – Iraq

[2]Department of Applied Sciences, University of Technology – Iraq

A R T I C L E   I N F O

Corresponding Author:
Aseel S. Jasim
as.18.10@grad.uotechnology.edu.iq

A B S T R A C T

In this work, we reported a study on the hydrothermal process for the preparation of TiO₂ NRs films on FTO substrate using two different solutions, the first consisting of (ethanol and titanium butoxide) and the second consisting of (HCl, DIW and titanium butoxide). The study of structural, morphological, optical and electrical properties helped to identify the characteristics of the TiO₂ films prepared with the different solvents. The first sample (TO1) exhibited an anatase phase crystal structure with an energy gap of (3.2 eV), while the second (TO2) showed a rutile phase with an energy gap of (3 eV). The (nanorod) morphology was observed in the (TO2) sample, while irregular grains were found in the (TO1) sample. Transmission measurements were performed to analyze the optical properties, which showed that both samples were transparent in the visible wavelength range, with the (TO2) sample with rutile phase exhibiting higher absorption coefficients. The activation energy was (0.0226) eV and (0.0643) eV for the two samples (TO1) and (TO2), respectively. The n-type conductivity was confirmed by Hall effect measurements for both samples. The highest conductivity (300.655) ($\Omega^{-1}.cm^{-1}$) and the highest carrier consternation (1.07355 $\times 10^{17}$) (cm^{-3}) were obtained for sample (TO1).

1. Introduction

Nanosized transition metal-based oxides have received a lot of attention in recent years, because of their ability to improve chemical, physical, and electrical properties. [1]. Titanium dioxide (TiO₂) belongs to the transition metal oxide family [2], it's commonly utilized as nanomaterial because of its attractive physicochemical properties, such as refractive index, non-toxicity, low cost, high photocatalytic activity, chemical stability, high dielectric constant, and good transmittance in the visible zone [3]. The three main crystallographic forms of TiO₂ are anatase (tetragonal) has a refractive index of n= 2.5, rutile (tetragonal) which being shaped at the elevated temperatures and possesses a refractive index (2.7), and brookite (orthorhombic) [4]. Each form differs in its structure and electronic characterizations depending on fabrication conditions and post-fabrication heat treatment [5-7], it also has different shapes, like nanotubes, nanorods, nanowire, nanosheets, and spider-web nanowires [8]. To synthesize TiO₂, many strategies have been used, including chemical bath deposition, electron beam evaporation,

hydrothermal method, liquid phase deposition method, DC magnetron sputtering, spray pyrolysis, sol-gel, and anodic oxidation [9]. TiO_2 was broadly utilized in a variety of applications, such as photovoltaic cells, integrated circuits, gas sensors, photocatalysis, dye-sensitized solar cells, and environmental devices [10]. The metal oxide compound TiO_2 has a large band gap (3.2 eV for the anatase and 3.0 eV for the rutile), limiting its solar spectrum absorption to the UV zone, which accounts for merely (4–5%) of solar radiation. Several strategies, including doping, dye sensitization surf was used for reducing its energy band gap and overcome this limitation, comprising the synthesis of the composite with else materials n-type semiconductor, dye sensitization surface adaptation, and doping, [11], and its conductivity rises as the O_2 loss degree in the lattice increases [12]. The structural, morphological, optical and electrical characteristics of the nanostructures can be tuned significantly by the ratio of reagents in the solvent, reaction temperature, calcination, and pH of the solution [13]. Aziz *et al*. [14] investigated the effect of different solvents on the morphology of TiO_2 1-dimensional nanostructures using the same precursor, it was discovered that different TiO_2 morphologies such as NRs, NBs, and NWs were obtained using different solvents such as HCl, NaOH, and HF under the same hydrothermal synthesis process. They also found that the prepared TiO_2 films exist in two phases (anatase and rutile) when HF and NaOH solvents are used, but only one phase (anatase) appears when HCl solvent is used. It was confirmed by Lu *et al*. [15] when they investigated the growth of TiO_2 NRs using more than five different solvents during the hydrothermal process and noted that the solvents' dielectric constants could be another crucial factor for determining the growth TiO_2 NRs. The films of TiO_2 films have been prepared on the substrates of FTO by the technique of hydrothermal using two different solvents, the first one using ethanol and the second using hydrochloric acid, and then studied the difference between their structural, morphological, optical, and electrical properties.

2. Method/ Experimental Work
2.1 Materials
The used materials in the present work include Tetra-n-butyl orthotitanate $[(CH_3CH_2CH_2CH_2O)_4Ti]$ (titanium Butoxide) (Sigma-Aldrich), Hydrochloric acid (37% Sigma-Aldrich), ethanol absolute from Scharlab S. L. (Spain), glycerol from Thomas Baker, acetone from Central Drug House (P) Ltd., isopropanol from Alpha Chemika, and deionized water from local markets.

2.2 Substrate Preparation
Fluorine-doped tin oxide-coated glass (FTO) glass slides (TEC 8 with a thickness of 600 nm from Techinstro) have been utilized as substrates in this study. Using equal ratios of the volume of isopropanol, acetone, and deionized water (DIW), the substrates were ultrasonically cleaned for (30) minutes, the substrates (2 cm × 5 cm) were then desiccated in air as well as located at an angle of 45˚ within a Teflon-closed vessel, and the conductive side was faced down.

2.3 Preparation of TiO_2 Films
Titanium dioxide NRs films have been prepared by using two methods. An aqueous solution of (2 mL) of Tetra-n-butyl orthotitanate (butoxide) $(C_{16}H_{36}O_4Ti)$ was added to (80 mL) of ethanol (C_2H_6O) under magnetic stirring for (30 min). And, the hydrothermal processing has been conducted at a temperature of 180˚C for a period of 24 h. Sample (TO1). An aqueous solution of (40 mL) of concentrate HCl acid was added to (40 mL) of (DIW) and stirred for about (10 min), then adding (1.33 mL) of Tetra-n-butyl orthotitanate (Ti $(RO)_4$) which was added dropwise and magnetically stirred for (10 min), and after that, the hydrothermal processing has been performed at a temperature of 180˚C for a period of 6 h. Sample (TO2). The preparation of sample (TO1) by using ethanol requires a long hydrothermal time (24h) and can't be prepared in a shorter amount of time, while (TO2) prepared by using (HCl) is typically prepared in a shorter hydrothermal time because longer time leads to films peeling out from FTO substrate. The simultaneous growth and dissolution processes may be what is causing the peeling off.

2.4 Tests
XRD technique has been employed for examining the crystal structure of prepared TiO_2 films using Shimadzu X-ray diffractometer with Cu Kα radiation (λ = 1.54060 Å) which was operated at (30 mA) as well as (40 kV). The range of (2θ) was (20°-90°) with a step scan of (0.02). The morphologies of prepared TiO_2 films were examined with a Field Emission-Scanning Electron Microscope (FE-SEM) (Inspect F50) Manufactured by FEI Company (USA). And, the optical properties have been measured using a UV–VIS spectrophotometer (Shimadzu) with a

wavelength ranging from (300–1100) nm. A Bruker ALPHA FTIR spectrometer with a range of 400-4000 cm^{-1} was used to obtain FT-IR spectroscopy. Beyond the depositing of Ag electrodes upon the film throughout a particular mask, the electrical resistance was measured directly with a digital multimeter. Hall Effect was measured using a system from Leybold GmbH Company (Germany).

3. Results and Discussion
3.1. Structural Properties
The pattern of the (XRD) of the produced TiO$_2$ films deposited upon the substrate of FTO fabricated via using a process of hydrothermal for sample (TO1) and sample (TO2) is depicted in Fig. 1. The XRD pattern display that both sample (TO1) and (TO2) films were TiO2 types with a tetragonal structure blended with both rutile and anatase phases. Peaks of diffraction were in good agreement with those of the rutile ICDD card (021-1276) and anatase ICDD card no. (046-1088). Sample (TO1) shows three peaks of anatase and two peaks of rutile which means that anatase is a major phase and rutile is a minor one, while sample (TO2) reveals five peaks of rutile and two anatase peaks which means that rutile is a major phase and anatase is a minor, as shown in Table 1. Anatase phase was obtained by using ethanol while rutile was obtained by using HCl. The photoelectrochemical activity of rutile and anatase is higher when both phases are present at the same time than when they are present separately [12- 16]. The biphasic TiO$_2$ structure enables the use of both rutile and anatase characteristics; the rutile possesses a higher refractive index as well as greater chemical steadiness than that of anatase [17], while the anatase has higher band gap energy and larger specific surface area.
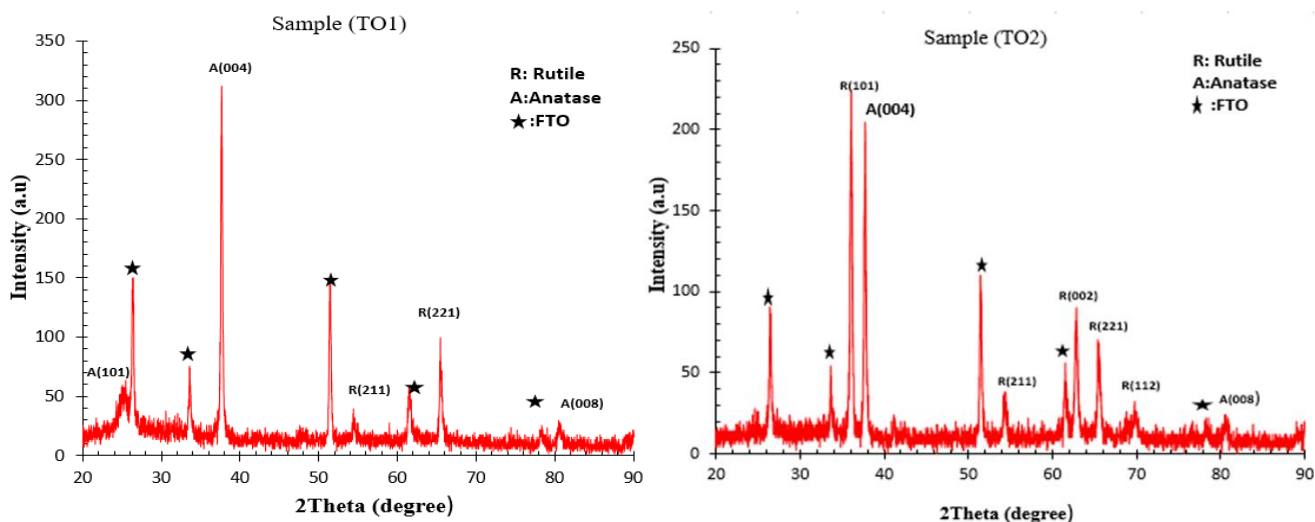

Figure 1: X-ray curve of prepared TiO$_2$ NRs for samples (TO1), and (TO2).

Table 1: (*hkl*) and (*2θ*) values for samples (TO1) and (TO2).

Sample (TO1)				Sample (TO2)			
Anatase phase		Rutile Phase		Rutile Phase		Anatase phase	
h k l	*2 θ*	*h k l*	*2 θ*	*h k l*	*2 θ*	*h k l*	*2 θ*
(101)	25.1238°	(211)	54.3814°	(101)	36.0350°	(004)	37.9953°
(004)	37.6508°	(221)	65.4228°	(211)	54.4064°	(008)	80.5984
(008)	80.5148°	-	-	(002)	62.7967°	-	-
-	-	-	-	(221)	65.4692°	-	-
-	-	-	-	(112)	69.7713°	-	-

The average crystallite size was estimated using Scherer's equation, Eq. (1) [18]:

$$D = k\,\lambda\,/\beta cos\,\theta\;(nm) \tag{1}$$

Where, λ = 1.54060 Å, β = Full Width Half Maximum (FWHM) in (rad.), k = 0.94, and θ = Diffracting angle Crystallite sizes of the sample (TO1) as well as (TO2) films are listed in Table 2.

Table 2: XRD parameters, strain, and domain size for samples (TO1) and (TO2).

Samples	$2(\theta)$ degree	hkl	β degree	Crystallite size (nm) Scherer's Eq	a=b (nm)	c (nm)	Strain along a	Strain along c
(TO1)	37.650	(004)	0.2268	39.6704	0.381	0.954	0.00749	0.00364
(TO2)	36.035	(101)	0.2902	37.958	0.454	0.295	-0.10106	-0.000304

Fig. 2 displays the images of FE-SEM for both samples (TO1) and (TO2). The whole surface of the FTO-glass substrate of (TO2) samples was uniformly covered with TiO_2 nanorods, as can be shown in the top view of the images. The nanorods' tips were spherical in form. The length of the nanorods was difficult to determine because the edges can't be seen clearly. In the (TO1) sample the FTO-glass substrate also was uniformly covered with TiO_2 films but with irregular grains. Nanorod morphology was obtained by using HCl while irregular grains were obtained by using ethanol.
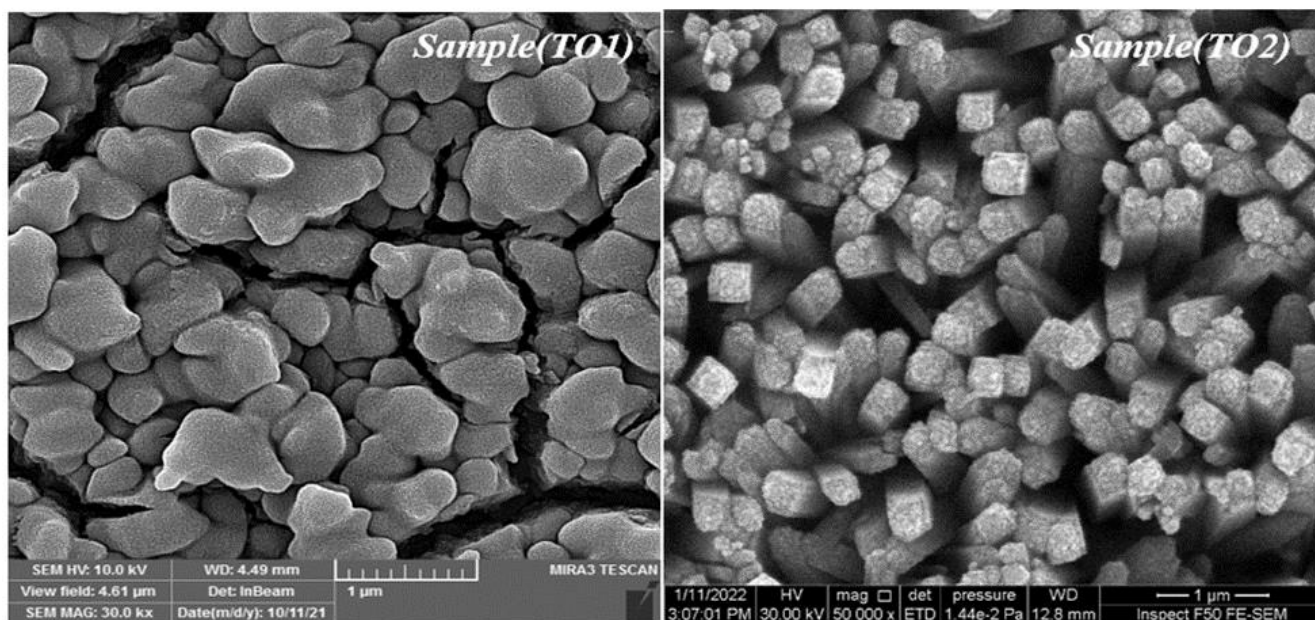
Figure 2: FE-SEM images of prepared TiO_2 NRs for samples (TO1) and (TO2).

The chemical compositions of TiO_2 nanorods for samples (TO1) and (TO2) are demonstrated via an energy-dispersive X-ray spectroscope (EDX), as displayed in Fig. 3. Fig. 3a evinces the existence of titanium (Ti), oxygen (O_2), Ti (79.29) percent O (20.71) percent. While Fig. 3b illustrates the EDX analysis of the sample (TO2) which also manifests that the prepared film comprises the (O_2) and (Ti) elements with ratios of approximately (57.90) and (22.50), correspondingly as illustrated in Table 3. Such values are consistent with the optimum stoichiometry of the sample.

The functional groups as well as the chemical composition of prepared TiO_2 films of samples (TO1) and (TO2) recorded under the wave number (400-4000 cm^{-1}) were examined using Fourier transform infrared spectroscopy (FTIR). As shown in Fig. 4a for sample (TO1), the peaks around (436.96 cm^{-1}) to (799.58 cm^{-1}) are due to stretching vibration of (Ti-O-Ti) and (Ti-O) [19], there is also a peak around (1053.72 cm^{-1}) due to (C-C) bond, the appearance of peaks around (1400.36 to 1686.53 cm^{-1}) denoted the presence of carboxylate which formed from ethanol precursor, and a peak at (2978.80 cm^{-1}) and (3668 cm^{-1}) is due to (-OH) stretching and bending vibration mode [22]. While, for the FTIR absorption spectrum for sample (TO2), Fig. 4b elucidated peaks around (431.89 to 821.96 cm^{-1}) representing (Ti-O) band and (Ti-O-Ti), respectively, there was also a broad band around (1400 to 35000 cm^{-1}) denoted the presence of carboxylate which formed from the titanium butoxide precursor [20], and finally, sample (TO2) had a peak around (3695.44 cm^{-1}) due to the (–OH) stretching mode.
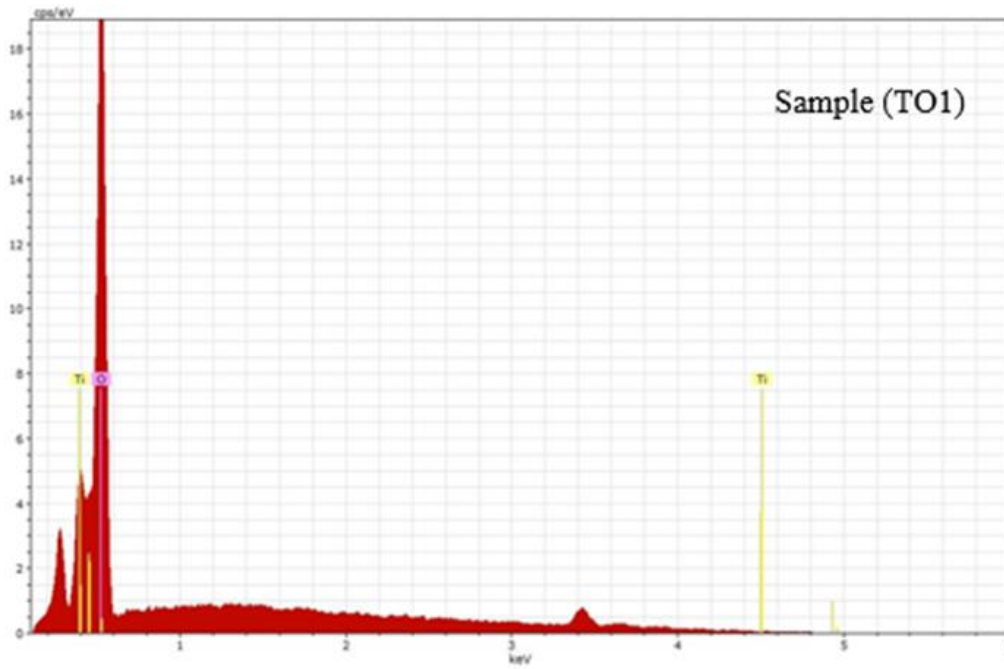
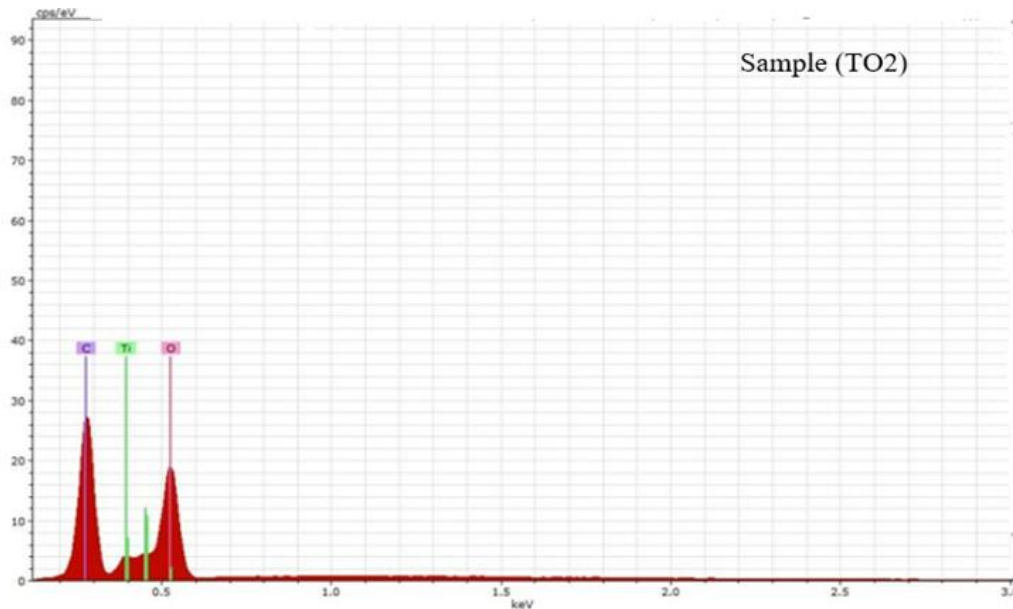**Figure 3a:** EDX patterns of prepared TiO_2 NRs for sample (TO1).

Figure 3b: EDX patterns of prepared TiO_2 NRs for samples (TO2).

Table 3: EDX spectrum of TiO_2 films for samples (TO1) and (TO2).

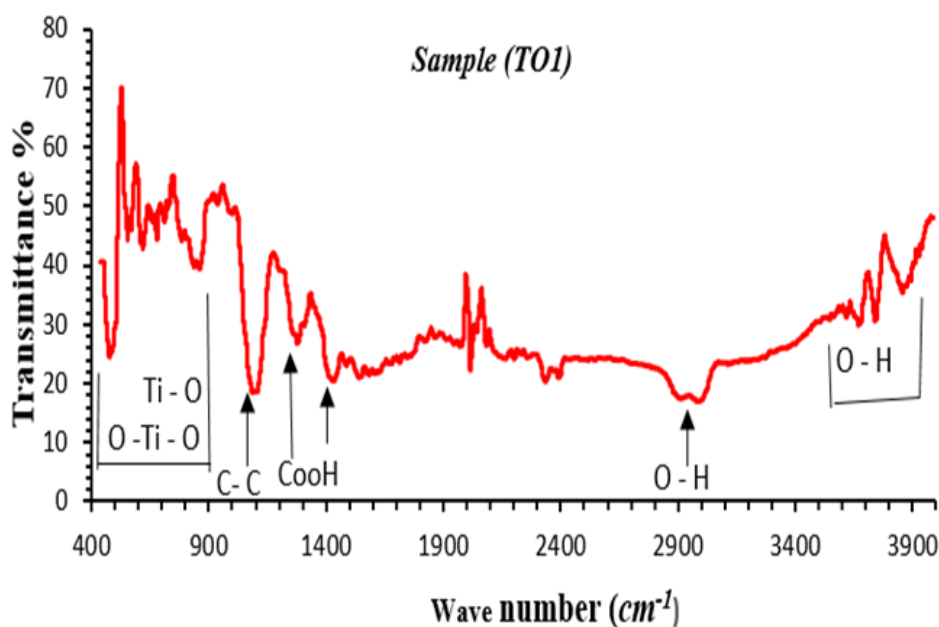| Sample (TO1)				Sample (TO2)			
Element	Line type	Weight%	Atomic%	Element	Line type	Weight%	Atomic%
O	Ka	65.13	79.29	O	La	48.11	57.90
Ti	La	43.87	20.71	Ti	Ka	41.38	22.50
-	-			C	Ka	10.51	19.60
		100.00	100.00			100.00	100.00

Figure 4a: FTIR spectrum of the produced TiO_2 NRs for sample (TO1).
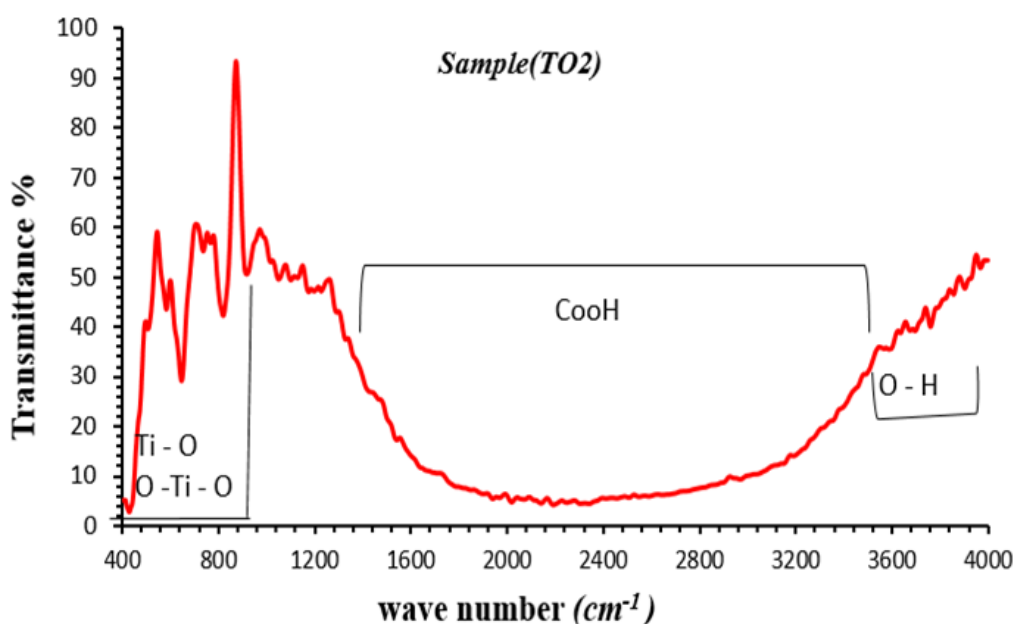
Figure 4b: FTIR spectrum of the produced TiO_2 NRs for sample (TO2).

3.2 Optical Properties

Fig. 5 portrays the transmittance spectra of prepared TiO_2 NRs for samples (TO1) and (TO2), the transmission increases with the increasing wavelength for both samples, sample (TO1) had the highest optical transmittance, whereas sample (TO2) had the lowest optical transmittance, and this is due to the fact that the sample (TO1) thickness being smaller than that for the sample (TO2), both samples were transparent in the visible wavelength range.
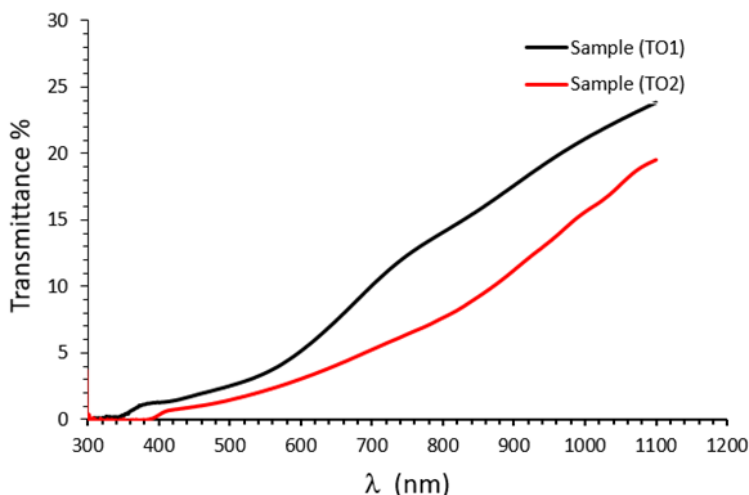
Figure 5: Transmittance spectra of prepared TiO_2 NRs for samples (TO1) and (TO2).

The absorption coefficient being calculated by applying Eq. (2) [21]:

$$\alpha = 2.303 \, A/t \tag{2}$$

Where: α is the coefficient of absorption, T is the thickness of film, and A is the absorbance. Coefficient of the absorption of the prepared TiO_2 NRs films for both samples (TO1) and (TO2) is exhibited in Fig. 6. As shown in this Figure, the films have a high absorption coefficient at short wavelengths and then decrease gradually at a long wavelength, and it is obviously seen that the sample (TO2) has absorption coefficient larger than sample (TO1) because (α) is inversely proportional to transmittance [22].
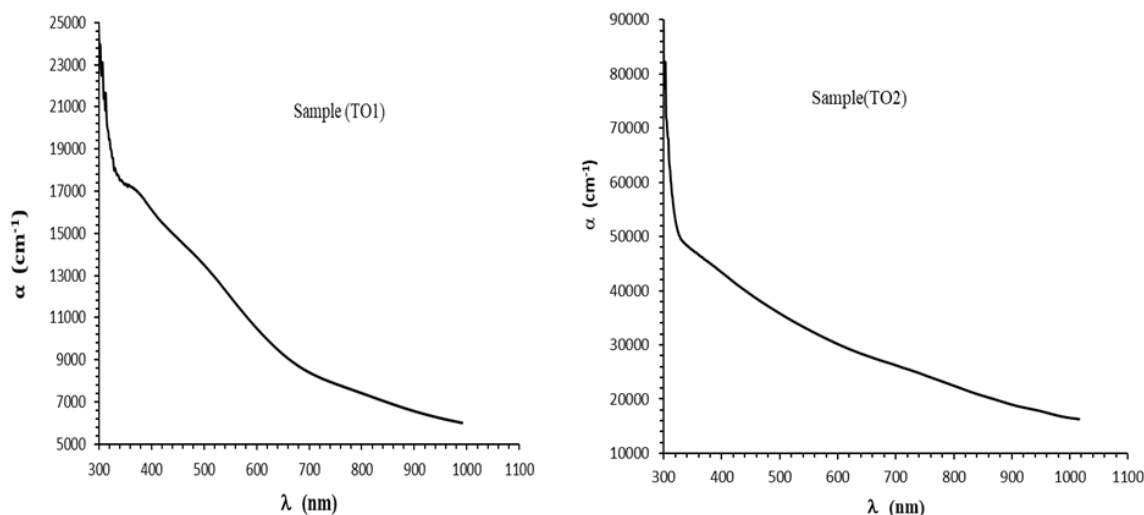

Figure 6: Coefficient of the optical absorption of prepared TiO_2 NRs for samples (TO1), (TO2).

The optical band gap was computed by using the following Eq. (3) [23]:

$$\alpha h v = \ constant \ (h v - E_g \ )^{(1/2)} \tag{3}$$

Where: α is the absorption coefficient, hv is the incident photon energy, and E_g is the Band gap.

Fig. 7 shows the plot of $(\alpha hv)^2$ versus photon energy (hv) which being utilized for estimating the optical band gap that was obtained to be (3.2 eV) for sample (TO1) which is equal to the anatase band gap. This result confirms the results of XRD (Fig. 1) which revealed that the dominating phase in sample (TO1) is anatase. While, the band gap

for sample (TO2) was (3 eV) which also confirms the results of XRD (Fig. 1) which depicted that the dominating phase in sample (TO2) is rutile.
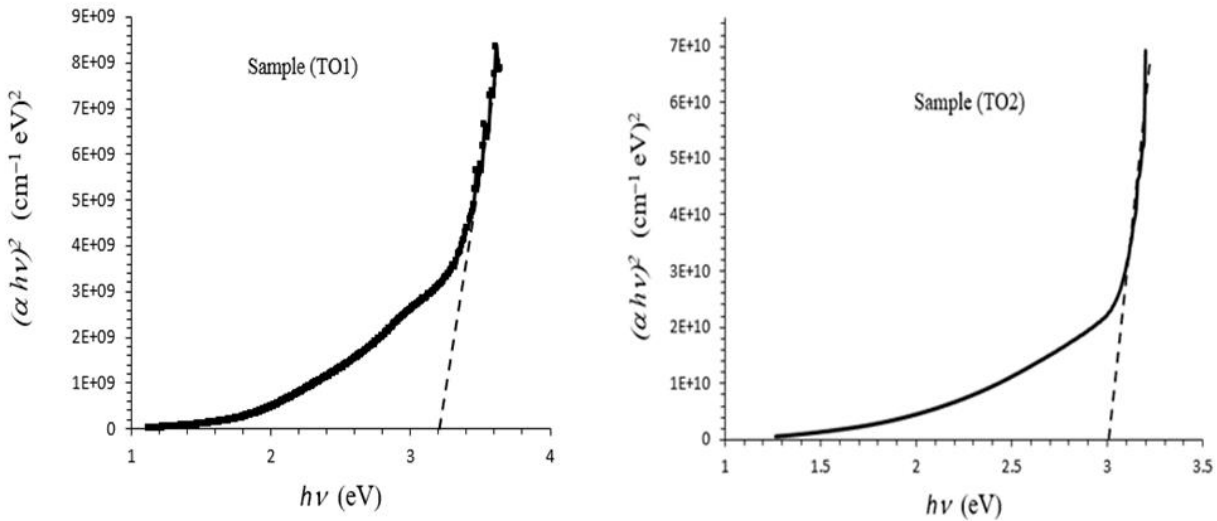

Figure 7: $(\alpha h\nu)_2$ as a function of (hv) of prepared TiO_2 NRs for samples (TO1), (TO2).

3.3 Electrical Properties

The values of activation energies (Ea) were calculated using the Arrhenius equation, as shown in Fig. 8 which depicts the variation of logarithm of DC conductivity (lnσ) for samples (TO1) and (TO2) as a function of reciprocal temperature (1000/T) in the thermal range of 35-150°C. And, it clearly shows that the increment in the temperature causes an increase in conductivity for both samples which they synthesized at different conditions. The fact that the conductivity increases with temperature indicates that the films are semiconductors. The activation energy was determined using Arrhenius Eq. (4) [24]:

$$\sigma = \sigma_0 ex(\frac{E_a}{(k_B\,T)}) \tag{4}$$

Where, (σ) is the medium conductivity, (σ_0) is a constant, (E_a) is the activation energy, (T) is the temperature, (K_b) is and Boltezmann constant. Activation energy was 0.0226 eV and 0.0643 eV for both sample (TO1) and (TO2), respectively, the demonstration was needed to activate the carriers for conduction.
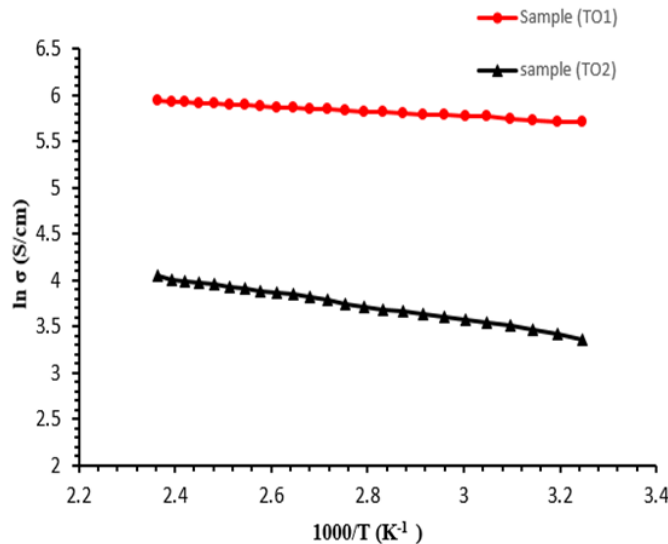

Figure 8: ln (σ) versus (1000/T) for TiO_2 NRs for samples (TO1) and (TO2).

Hall effect studies were carried out on TiO_2 NRs to ascertain the predominant charge carrier type, mobility, and concentration. The linear relation between the Hall voltage (VH) and the current (I) had a negative slope as shown in Fig. 9, indicating that the TiO_2 samples were n-type, which is due to the oxygen vacancy [25]. The Hall Effect coefficients are listed in Table 4 for both samples.
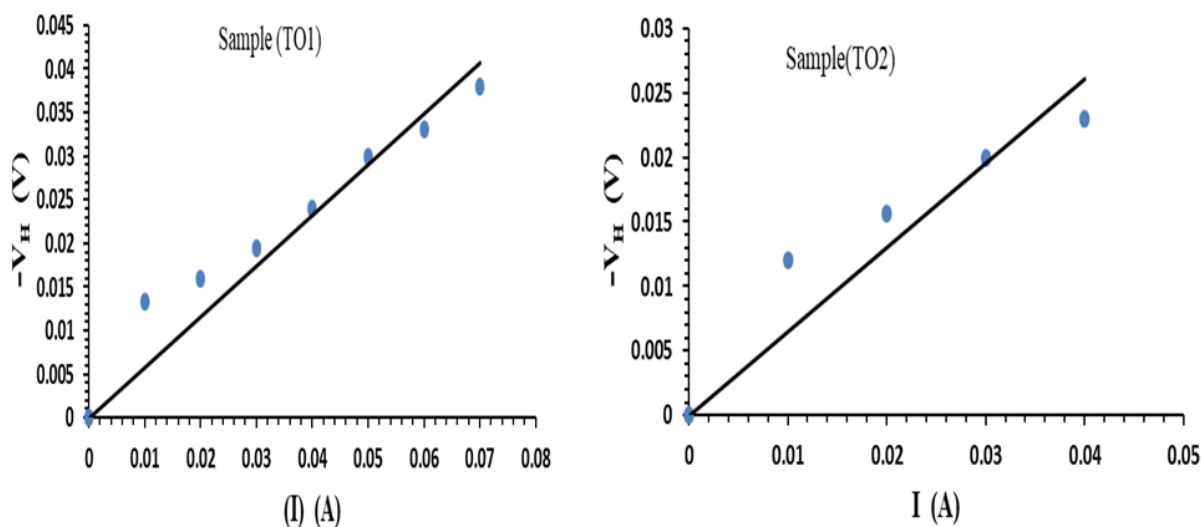

Figure 9: Hall voltage as a function of current for TiO_2 NRs for samples (TO1) and (TO2)

Table 4: Hall Effect parameters for samples (TO1) and (TO2).

Samples	$\Delta VH/\Delta I$	$RH(cm^3/C)$	$nH\ (cm^{-3})$	$\mu H(cm^2/v.s)$	$\sigma RT\ (\Omega^{-1}.cm^{-1})$	$\rho\ (\Omega.cm)$
(TO1)	-0.464	58.218	1.07355E+17	17503.571	300.655	0.0033
(TO2)	-0.374	64.552	9.68206E+16	1864.434	28.882	0.0346

4. Conclusions

The findings of the research presented in this paper lead to the following conclusions. TiO_2 films with crystallite sizes 39.67 nm and 37.95 nm were successfully prepared for samples (TO1) and (TO2), respectively by using the hydrothermal method and different solvents. The domain phase in the sample (TO1) was the anatase phase, while rutile was the domain phase in the sample (TO2) with nanorode morphology for both samples. Sample (TO1) has higher transmittance, whereas sample (TO2) has a higher absorption coefficient. Both samples have n-type conductivity owing to the O_2 vacancies, and their conductivity increases as the temperature increases which indicates that both films were semiconductors.

Conflict of Interest

The authors declare that they have no conflict of interest.

References

[1] J. Jeevanandam, A. Barhoum, Y. S. Chan, A. Dufresne, and M. K. Danquah, "Review on nanoparticles and nanostructured materials: History, sources, toxicity and regulations," *Beilstein J. Nanotechnol.*, vol. 9, no. 1, pp. 1050–1074, 2018.

[2] Z. N. Ameel, A. J. Al-Hussaini, Haider, and Ji. H.M., "Review on: Titanium dioxide applications," *Energy Procedia*, vol. 157, pp. 17–29, 2019.

[3] S. M. H. Al-Jawad, M. R. Mohammad, and N. J. Imran, "Effect of electrolyte solution on structural and optical properties of TiO_2 grown by anodization technique for photoelectrocatalytic application," *Surf. Rev. Lett.*, vol. 25, no. 4, pp. 1–16, 2018.

[4] T. Touam *et al.*, "Low loss sol-gel TiO_2 thin films for waveguiding applications," *Coatings*, vol. 3, no. 1, pp.

49–58, 2013.

[5]   I. F. Mironyuk, L. M. Soltys, T. R. Tatarchuk, and K. O. Savka, "Methods of titanium dioxide synthesis (review)," *Phys. Chem. Solid State*, vol. 21, no. 3, pp. 462–477, 2020.

[6]   R. Dholam, N. Patel, M. Adami, and A. Miotello, "Hydrogen production by photocatalytic water-splitting using Cr- or Fe-doped TiO$_2$ composite thin films photocatalyst," *Int. J. Hydrogen Energy*, vol. 34, no. 13, pp. 5337–5346, 2009.

[7]   M. Zhang, T. Chen, and Y. Wang, "Insights into TiO$_2$ polymorphs: Highly selective synthesis, phase transition, and their polymorph-dependent properties," *RSC Adv.*, vol. 7, no. 83, pp. 52755–52761, 2017.

[8]   S. M. H. Al-jawad and M. M. Ismail, "Characteristics of Ni-doped TiO$_2$ nanorod array films," 2020.

[9]   S. Hashim, K. Hassoon, and O. Salman, "Structural Properties of Fe Doped TiO$_2$ Nanorods Prepared by Low Cost Hydrothermal Method," *Eng. Technol. J.*, vol. 38, no. 3B, pp. 177–183, 2020.

[10]   I. Hasan, K. Khashan, and A. Hadi, "Study of the Effect of Laser Energy on the Structural and Optical Properties of TiO$_2$ NPs Prepared by PLAL Technique," *J. Appl. Sci. Nanotechnol.*, vol. 2, no. 1, pp. 11–19, 2022.

[11]   P. Malliga, J. Pandiarajan, N. Prithivikumaran, and K. Neyvasagam, "Influence of Film Thickness on Structural and Optical Properties of Sol – Gel Spin Coated TiO$_2$ Thin Film," *IOSR J. Appl. Phys.*, vol. 6, no. 1, pp. 22–28, 2014.

[12]   S. M. H. Al-jawa, "Structural and Optical Properties of Core – Shell TiO $_2$ / CdS Prepared by Chemical Bath Deposition," *J. Electron. Mater.*, 2017.

[13]   R. Saleh, O. Salman, and M. Dawood, "Physical Investigations of Titanium Dioxide Nanorods Film Prepared by Hydrothermal Technique," *J. Appl. Sci. Nanotechnol.*, vol. 1, no. 3, pp. 32–41, 2021.

[14]   T. I. O. Nanoparticles, "Effect of Different Organic Solvents and Annealing Temperatures on Optical Property of," vol. 1, no. 1, pp. 61–64, 2014.

[15]   W. J. Aziz, R. S. Sabry, and A. K. Jarallah, "Effect shapes of nanorods, nanowires and nanobelts TiO$_2$ on the degradation of MB photo catalyst.," J. Phys. Conf. Ser., vol. 1032, no. 1, 2018.

[16]   X. Lu, M. Li, S. Hoang, S. L. Suib, and P. X. Gao, "Solvent effects on the heterogeneous growth of TiO$_2$ nanostructure arrays by solvothermal synthesis," Catal. Today, vol. 360, pp. 275–283, 2021.

[17]   A. Prathan *et al.*, "Controlled Structure and Growth Mechanism behind Hydrothermal Growth of TiO$_2$ Nanorods," *Sci. Rep.*, vol. 10, no. 1, pp. 1–11, 2020.

[18]   O. Secundino-Sánchez, J. Diaz-Reyes, J. F. Sánchez-Ramírez, and J. L. Jiménez-Pérez, "Structural and optical characterization of the crystalline phase transformation of electrospinning TiO$_2$ nanofibres by high temperatures annealing," *Rev. Mex. Fis.*, vol. 65, no. 5, pp. 459–467, 2019, doi: 10.31349/RevMexFis.65.459.

[19]   V. M. Gaikwad, "Related Papers," *Over Rim*, pp. 191–199.

[20]   S. H. Nam, S. J. Cho, and J. H. Boo, "Growth behavior of titanium dioxide thin films at different precursor temperatures," *Nanoscale Res. Lett.*, vol. 7, pp. 1–6, 2012.

[21]   O. N. Salman, M. M. Ismail, and T. H. Ali, "Growth Time Influence on Optical and Electrical Properties of TiO$_2$ Nanorods Prepared via Hydrothermal Method," *J. Phys. Conf. Ser.*, vol. 2114, no. 1, 2021.

[22]   S. M. H. Al-Jawad, A. K. Elttayf, and A. S. Saber, "Studying Structural, Optical, Electrical, and Sensing Properties of Nanocrystalline SnO$_2$:Cu Films Prepared by Sol-Gel Method For CO Gas Sensor Application at Low Temperature," *Surf. Rev. Lett.*, vol. 24, no. 8, 2017.

[23]   M. H. Shinen, S. A. A. Alsaati, and F. Z. Razooqi, "Preparation of high transmittance TiO$_2$ thin films by sol-gel technique as antireflection coating," *J. Phys. Conf. Ser.*, vol. 1032, no. 1, 2018.

[24]   O. N. Salman, M. O. Dawood, A. K. Ali, D. S. Ahmed, and K. I. Hassoon, "Low-cost synthesis of ZnO nano thin films by electrochemical deposition," *Dig. J. Nanomater. Biostructures*, vol. 12, no. 3, pp. 719–726, 2017.

[25]   K. H. Aboud, N. Jamal Imran, and S. M. H. Al-Jawad, "Structural, Optical and Morphological Properties

Cadmium Sulfide Thin Films Prepared by Hydrothermal Method," *J. Appl. Sci. Nanotechnol.*, vol. 1, no. 2, pp. 49–57, 2021.

[26]   N. Ali, A. Taha, and D. Ahmed, "Characterization of Treated Multi-Walled Carbon Nanotubes and Antibacterial Properties," *J. Appl. Sci. Nanotechnol.*, vol. 1, no. 2, pp. 1–9, 2021.

[27]   S. L. K., S. Roy, and K. U. Rao, "Evaluation of Activation Energy (Ea) Profiles of Nanostructured Alumina Polycarbonate Composite Insulation Materials," *Int. J. Mater. Mech. Manuf.*, vol. 2, no. 1, pp. 96--100, 2014.

[28]   S. Wang *et al.*, "Titanium-defected undoped anatase TiO_2 with p-type conductivity, room-temperature ferromagnetism, and remarkable photocatalytic performance," *J. Am. Chem. Soc.*, vol. 137, no. 8, pp. 2975–2983, 2015.